ADVANCED MATERIALS
www.advmat.de

The Relation between Chemical Bonding and Ultrafast Crystal Growth

Tae Hoon Lee and Stephen R. Elliott**

Glasses are often described as supercooled liquids, whose structures are topologically disordered like a liquid, but nevertheless retain short-range structural order. Structural complexity is often associated with complicated electron-charge distributions in glassy systems, making a detailed investigation challenging even for short-range structural order, let alone their atomic dynamics. This is particularly problematic for lone-pair-rich, semiconducting materials, such as phase-change materials (PCMs). Here, this study shows that analytical methods for studying bonding, based on the electron-charge density, rather than a conventional atomic pair-correlation-function approach, allows an in-depth investigation into the chemical-bonding network, as well as lone pairs, of the prototypical PCM, $Ge_2Sb_2Te_5$ (GST). It is demonstrated that the structurally flexible building units of the amorphous GST network, intimately linked to the presence of distinctly coexisting weak covalent and lone-pair interactions, give rise to cooperative structural-ordering processes, by which ultrafast crystal growth becomes possible. This finding may universally apply to other PCMs.

The absence of long-range structural order is the central structural signature of amorphous materials, although, in most cases, their short-range order, and sometimes medium-range order, is preserved.[1] Amorphous covalent structures have, therefore, long been described as a network of connected basic structural units.[2] Except for simple (stoichiometric) compounds, however, it becomes challenging comprehensively to understand their structures, primarily due to the complex chemical-bonding nature between constituent elements. A particular class of materials, belonging to this category, are the lone-pair-rich, amorphous chalcogenides, in particular, phase-change materials (PCMs), which have attracted great attention recently, due to their unique properties and corresponding diverse practical applications, such as for nonvolatile memory[3–5] or neuromorphic computing devices.[6,7] Among various material systems, the prototypical PCM is the ternary compound $Ge_2Sb_2Te_5$ (GST).[3]

Dr. T. H. Lee, Prof. S. R. Elliott
Department of Chemistry
University of Cambridge
Lensfield Road, Cambridge CB2 1EW, UK
E-mail: thl32@cam.ac.uk; sre1@cam.ac.uk

The ORCID identification number(s) for the author(s) of this article can be found under http://dx.doi.org/10.1002/adma.201700814.

DOI: 10.1002/adma.201700814

Applications of PCMs make use of their ultrafast crystallization behavior and large electronic (or optical) contrast between metastable crystalline and amorphous phases.[3] Recent advances in first-principles computer modeling have extended its usage for studying amorphous PCMs and established its usefulness for understanding their structure and crystallization behavior under various conditions at the atomic scale;[8–10] unambiguous experimental observations are very limited in this case.[11] In spite of its significance, however, the link between the amorphous structure and dynamical properties still remains obscure. Usually, the coordination number (CN) of atoms is investigated in terms of pair-correlation functions, i.e., the number of neighbors within a certain distance from an origin atom. This conventional method takes no consideration of the electronic charge distribution in the system, although the latter actually determines the bonding network of amorphous covalent materials; as a consequence, atoms with similar interatomic distances can have very different chemical-bonding configurations, depending on their local environment. The presence of chalcogen elements possessing "lone pairs" of electrons escalates this structural complexity, as lone pairs can significantly affect the strength of nearby bonds[12] and the geometry of the local coordination in general.[13] A proper understanding of the nature, and dynamics, of chemical bonds and lone pairs, therefore, is a fundamental requirement for comprehending the unique properties of PCMs. Until recently, however, very few studies have systematically explored this crucial issue, except for simple bonding configurations or lone pairs in amorphous PCMs.[14–17]

Here, we address congruently the problem of atomic structure, and crystal-growth kinetics, of GST from the static, and dynamical, behavior of local atomic structures. In doing so, we consider the electronic-charge distribution via ab initio molecular-dynamics (AIMD) simulations, along with analytic methods based on local electronic structures, revealing new findings, concealed in the conventional approach. We show that, in spite of its complicated local bonding structure, the network structure of amorphous GST (a-GST) can be comprehensively described in terms of well-defined basic structural units. The mechanism of ultrafast crystal growth in a-GST at the atomistic scale is unveiled from the interplay between the existence of "structurally flexible" units and fast crystal-growth kinetics.

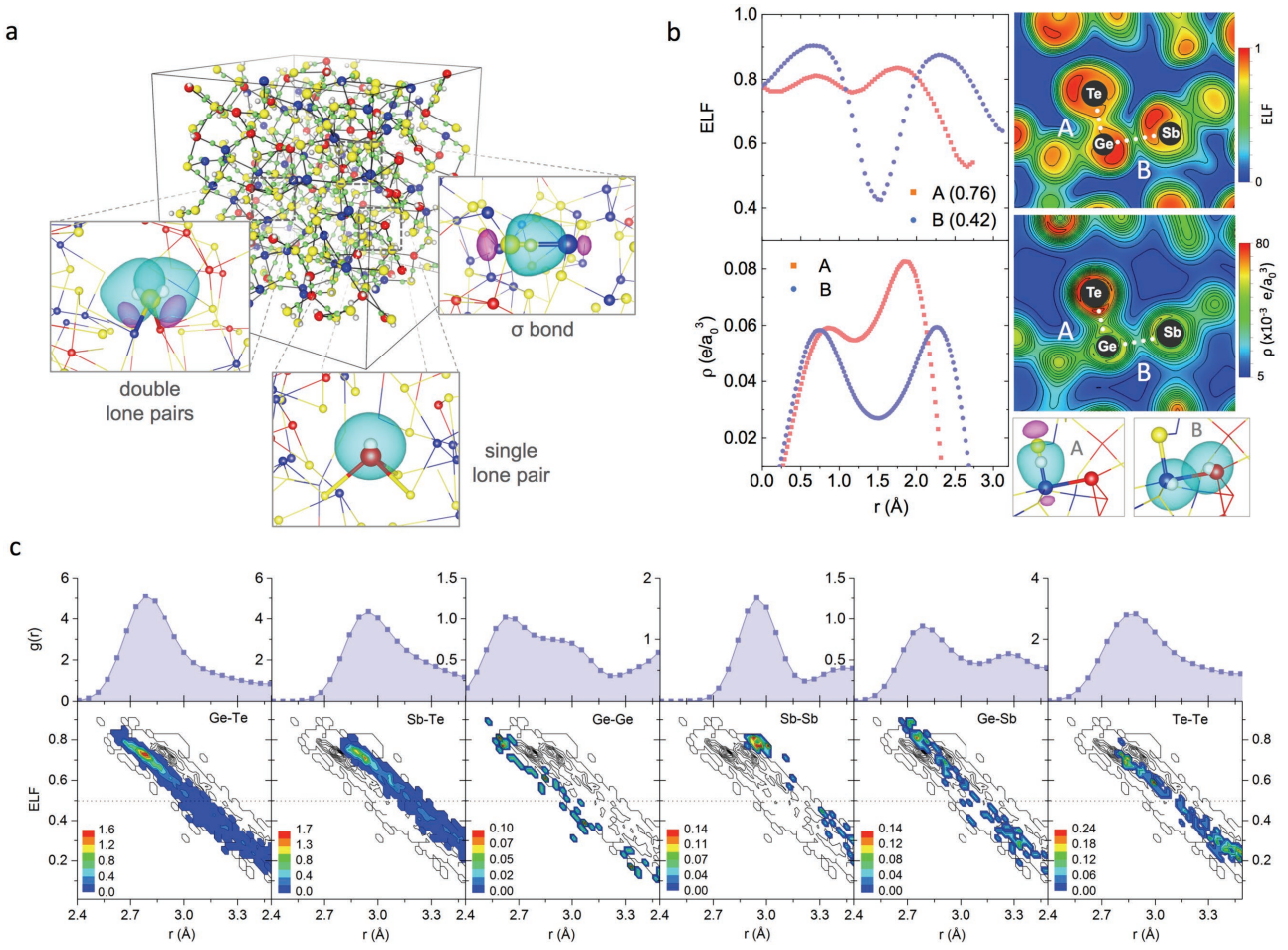

Figure 1. First-principles methods for analyzing chemical bonds and lone pairs. a) Maximally localized Wannier functions (MLWFs). The spatial distribution of atoms of Ge (blue), Sb (red), and Te (yellow) in an amorphous GST model are shown with the MLWF centers for bonds (green) and lone pairs (white). Examples of isosurface-contour plots of MLWFs (cyan for positive and purple for negative values) are also illustrated for a σ bond, single lone pair, and double lone pairs. b) Electron-localization functions (ELFs) and charge densities (ρ). The line profiles of ELF (left upper) and ρ (left lower) along the bond paths A (red) and B (blue) are depicted (Ge at $r = 0$), together with the 2D contour plots for ELF (right upper) and ρ (right middle). The minimum ELF value along each bond path (ELF_{bond}) for the bond paths A (Ge—Te distance = 2.8Å) and B (Ge—Sb distance = 3.1Å) are shown in the parentheses. The isosurface-contour plots (same color coding as in (a)) of MLWFs are displayed with MLWF centers (right bottom). c) ELF_{bond} versus interatomic distance. The radial distribution functions (upper panels) and the contour plots for the distribution of ELF_{bond} values (lower panels) are shown. The scale for the ELF contour plots indicates the range from high (red) to low (blue) population densities.

To characterize an amorphous network in terms of bonds and lone pairs, we employed both the electron localization function (ELF)[18] and maximally localized Wannier functions (MLWFs) (see the Supporting Information),[19] combined with AIMD using the Vienna Ab initio Simulation Package.[20] A significant feature of the MLWF approach is that the overall charge density can be represented by a set of localized Wannier-function charge centers (WFCs), allowing a convenient, simple description of electronic states.[19] **Figure 1**a shows the distribution of atoms and WFCs in an amorphous GST model (see the Supporting Information). Two types of MLWFs, representing either bonding or lone pairs shared by two electrons, were identified according to their shapes and positions, and their typical isosurface shapes are shown. As indicated from the complicated distribution of WFCs, however, a certain ambiguity can arise in determining whether each WFC corresponds to either a chemical bond or lone pair,[21] indicating the need for another approach to complement the WFC results.

Since the ELF indicates the probability of finding electron pairs,[18] paired electrons in a shared covalent bond or in a lone pair can be similarly investigated.[22] In particular, by searching for the minimum ELF value along a bond path (ELF_{bond}),[14] one can measure the relative degree of the covalent-bond interaction (or strength) in terms of electron pairing. Indeed, ELF_{bond} displays an almost linear relationship with the atomic distance for every type of atom pair in GST (Figure 1 c), supporting this interpretation; further evidence will be given later. A noticeable variance in ELF_{bond} for each bond distance, however, means that the conventional atomic-distance-based approach cannot fully capture these subtle differences, rationalizing the need for considering ELF or MLWF analyses in investigating chemical-bonding properties. We have chosen the signature of significant covalent bonding to be $ELF_{bond} > 0.5$, this lower-bound ELF_{bond}

value corresponding to that of a uniform electron gas.[18] The relationships among the values of ELF_{bond}, charge densities at the bond critical point (ρ_{BCP}),[23] and WFCs are shown in Figure 1b for the case of GST, with the following observations: i) ELF_{bond} scales with ρ_{BCP}; ii) the formation of a covalent bond can be represented by a high ELF_{bond} value (>>0.5) and a single WFC between two adjacent atoms—denoted as a bonding WFC; iii) a very small ELF_{bond} value (<<0.5), or two WFCs (each belonging to two separate atoms), indicates marginal chemical interactions, and the corresponding WFCs are classified as non-bonding, lone-pair WFCs; and iv) intermediate range ELF_{bond} values (≈0.5) correspond to weak chemical interactions, with a single bonding WFC for a pair of atoms.

Building on the above findings, the basic structural units, which fully describe the network structure of amorphous GST, could be determined, based on the number of bonding and lone-pair WFCs of the corresponding central atoms (**Figure 2**a,b). Various types of structural units were identified. For brevity, we introduce a concise notation; for example, Ge(3,1) denotes a Ge-centered structural unit which has three-fold coordination (the first number in parentheses) and a single lone pair (the second number). The observed structural units in glassy GST then are: Ge(3,1) (60%), Ge(4,0) (25%), and Ge(4,1) (12%) for Ge-centered units; Sb(3,1) (58%), Sb(4,1) (34%), and Sb(5,1) (5%) for Sb-centered units; and Te(2,2) (44%) and Te(3,1) (53%) for Te-centered units, with the population of each unit (as a percentage) given in parentheses (Figure 2b). The use of a higher minimum ELF_{bond} value to define bonds slightly decreases the population of structural units with high CNs (see **Figure 3**a). Minor-population structural units (<1%) are not shown here. (3,1)-type units with a trigonal pyramidal geometry were observed for all types of atoms, while (4,1)-type units are observed mostly for Ge and Sb atoms, and have a "see-saw" molecular geometry, i.e., two axial and two equatorial bonds with a lone pair residing at the equatorial position. The square-pyramidal (5,1)-type unit is observed mainly for Sb atoms. Since

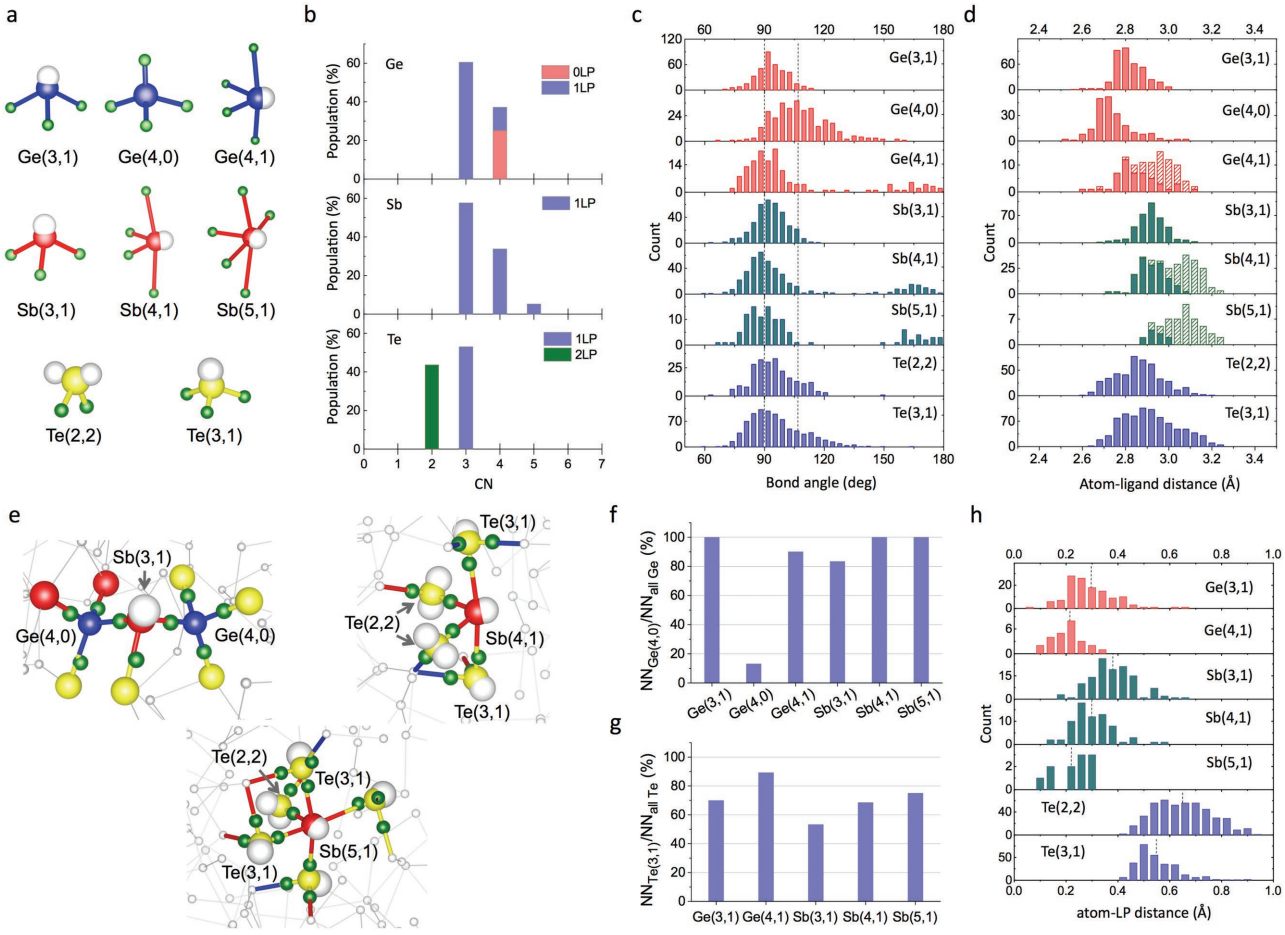

Figure 2. Structural characteristics of basic structural units and their connections. a) Molecular geometries of structural units identified in GST, M(*m*,*n*), where M is the central atom (Ge, Sb, Te), *m* is the nearest-neighbor coordination number (CN), and *n* is the number of lone pairs (same color coding as in Figure 1a). b) Relative populations of structural units as functions of their CNs and the number of lone pairs. c) Bond-angle distributions (BADs). d) Bond-length distributions. For (4,1)- or (5,1)-type units, the shaded area corresponds to equatorial or central bonds, respectively, while the hatched area corresponds to axial bonds. e) Examples of preferential connections between structural units. f) Ratio (as a percentage) of the total number of (4,0)-type Ge nearest neighbors (NNs) to the total number of all types of Ge NNs with the denoted structural unit. g) Ratio (as a percentage) of the total number of (3,1)-type Te NNs to the total number of all types of Te NNs with the denoted structural unit. h) Distribution of the distance between the central atom and their lone-pair MLWF centers.

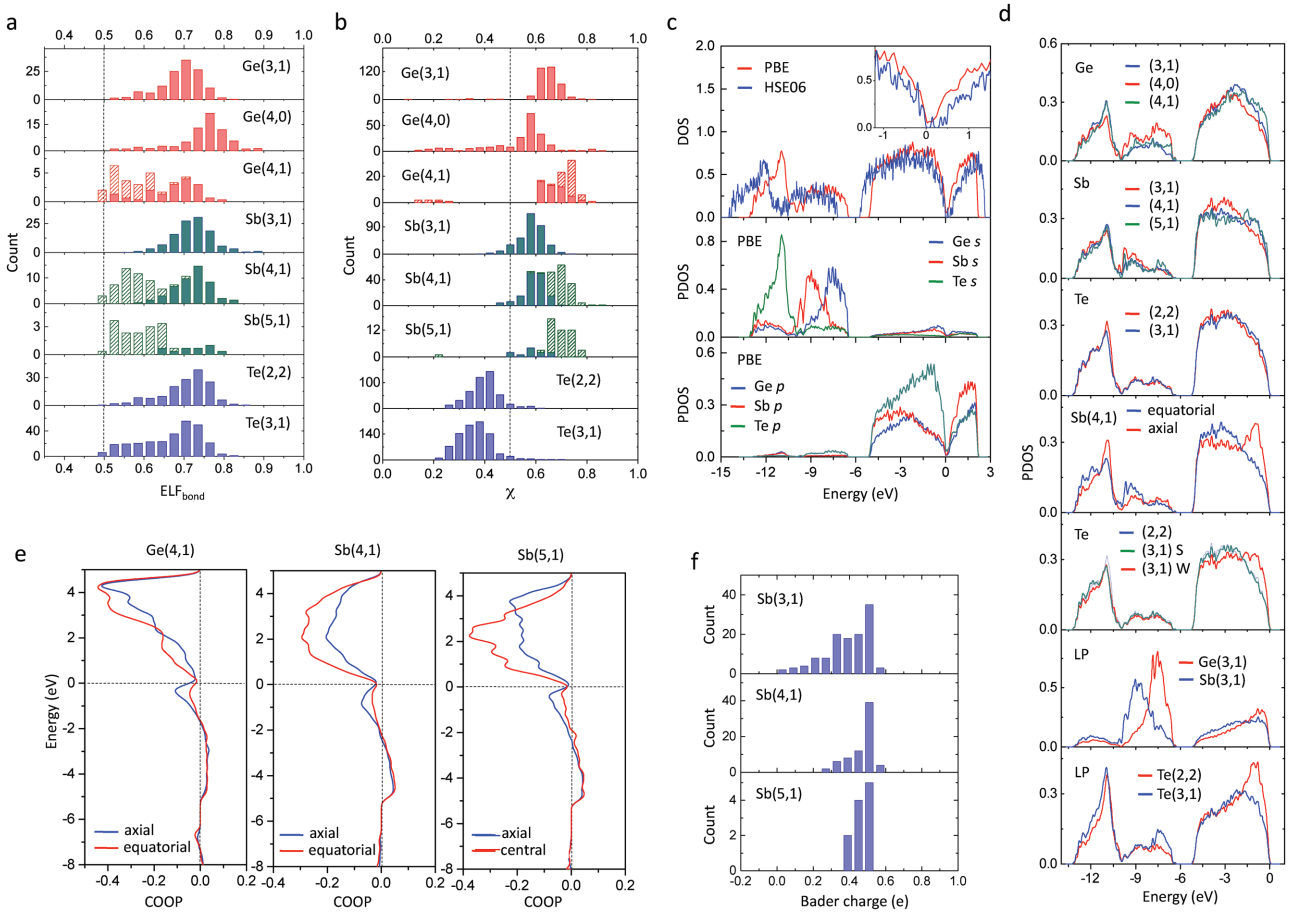

Figure 3. Nature of chemical bonds and lone pairs. a) Distribution of ELF_{bond} values. b) Relative position of bond MLWF centers along the bond path between the central atom and their ligands. The relative distance from the central atom to each bond MLWF center (here the distance to the ligand is normalized to unity) is expressed as χ. c) Electronic density of states (DOS). The DOSs (top) computed with PBE or HSE hybrid functionals are displayed with the partial DOSs (computed with PBE) for the s (middle) or p orbitals (bottom) of each type of atom. The Fermi level is set at zero energy. d) Partial DOSs (PDOSs) projected onto the bond or lone-pair MLWFs. The PDOSs are shown for: the bond MLWFs for each type of structural unit (top three panels); the equatorial- or axial-bond MLWFs for Sb(4,1) (fourth panel); the MLWFs for weak (W), and the remaining two strong (S), bonds for Te(3,1) units, along with the bond MLWFs for Te(2,2) units; and the lone-pair MLWFs for each type of structural unit (bottom two panels). e) Crystal-orbital-overlap populations (COOPs) computed for axial, or equatorial (or central), bonds. f) Bader charges for Sb atoms.

the number of electrons involved in forming bonds or lone pairs exceeds eight per atom in their Lewis structures, the (4,1) and (5,1) units of Ge or Sb atoms can be regarded as hypercoordinated units. As shown in Figure 2d, axial bonds (hatched) have, in general, longer bond distances than equatorial (or central) bonds (shaded) for hypercoordinated units. All structural units show a peak at ≈90° in their bond-angle distributions (BADs), except for the tetrahedral Ge(4,0) unit (≈109°), and the large bond angles (>150°) for hypercoordinated units are between two axial bonds (Figure 2c). It is worth noting that the geometries of all the structural units in Figure 2a largely conform to the prediction of valence-shell electron-pair repulsion theory[24] (see the Supporting Information). Kolobov et al.[15] have discussed the lone-pair formation of trigonal pyramidal Ge units in GeTe, and their possible role in crystallization.

In forming the bonding network, structural units showed a preferential coordination with certain types of other units (Figure 2f,g). All structural units possess a certain proportion of "wrong" bonds, i.e., Ge—Ge, Ge—Sb, Sb—Sb, or Te—Te bonds. In particular, when Ge or Sb atoms form a bond with other Ge atoms, they are preferentially coordinated to tetrahedral Ge(4,0) units; however, Ge(4,0) units seem to avoid each other (Figure 2f). Approximately 30% (the highest among other units) of Ge(4,0)-forming bonds are wrong bonds, and the lowest percentage of wrong bonds was found for Ge(3,1) units (≈4%) (Figure S1, Supporting Information). Moreover, as Ge and Sb units are coordinated with more than three atoms, Te(3,1) is more preferred as a ligand than Te(2,2) (Figure 2g), indicating that the axial bonds of hypercoordinated units prefer Te(3,1) rather than Te(2,2) units. Some of these features in preferential connections are illustrated in Figure 2e. Apart from the above findings, no other noticeable trends between bonding types and preferential coordinations were identified.

The presence of diverse structural units in a-GST is induced by a broad range of electronic configurations that each central atom can take. We found that each electronic configuration has its unique features. First, to understand their peculiar bonding characteristics, we compared the distribution of

values of ELF_{bond} (Figure 3a). The ELF_{bond} distributions for (3,1) units, and for the equatorial (or central) bonds of hypercoordinated units, reveal a close similarity in terms of their peak positions (≈0.7) and shapes. However, the axial bonds of hypercoordinated units show ELF_{bond} distributions well separated from others, with the center of the distribution at a much lower ELF_{bond} value (≈0.55). The same trend is also observed in their bond distance (Figure 2d) and the position of WFCs (Figure 3b). These distinctive features suggest that axial bonds can be differentiated from other bonds. In terms of ELF_{bond} values, axial bonds tend to have weaker covalent interactions than do other bonds; this is also inferred from their more delocalized MLWFs (Figure S2, Supporting Information). To study this further, we compared the crystal-orbital-overlap population (COOP).[25] As shown in Figure 3e, axial bonds have a more antibonding nature (i.e., a negative COOP value) near the Fermi level (E_f) than equatorial or central bonds. It is, thus, the antibonding states near E_f that cause the axial bonds to be weaker, and the bonding distance to be larger, than for other bonds. Tetrahedral Ge(4,0) units also show distinct features, i.e., the highest ELF_{bond} values (Figure 3a), the shortest bond distances (Figure 2d), and the most localized MLWFs (Figure S3, Supporting Information). Together with the smaller polarity (explained later), all these observations point to relatively strong covalent-bonding interactions between Ge(4,0) units and their neighbors, in stark contrast to the axial bonds of hypercoordinated units.

More detailed insights into bonding, and lone pairs, can be gained from the partial electronic density of states (PDOSs) projected onto the bond ($PDOS_{BO}$) or lone-pair ($PDOS_{LP}$) MLWFs (Figure 3d). Here, we consider PDOSs obtained from the less computationally intensive Perdew–Burke–Ernzerhof (PBE) functional,[26] rather than the Heyd–Scuseria–Ernzerhof (HSE) hybrid functional,[27] for better statistics, in spite of the better bandgap description of the latter (top panel in Figure 3c); the general conclusions are the same for both cases (Figure S4, Supporting Information). The averaged $PDOS_{BO}$ (upper two panels in Figure 3d) indicates that most of the covalent bonding possesses mainly cation (Ge or Sb) p and anion (Te) s-p hybridized-orbital character, corresponding to the cation BAD peak at ≈90° (Figure 2c). The formation of lone pairs for Te atoms through s-p mixing has seldom been documented in phase-change materials.[15,28] The tetrahedral bonding of Ge(4,0) units, on the other hand, contains more Ge 4*s* (with less p near the Fermi level) orbital components than the others, indicative of sp^3-type hybridized Ge orbitals, corresponding to the BAD peak at ≈109° (Figure 2c). The axial bonds are differentiated by the extra antibonding DOS near the Fermi level (Figure 3e), which also distinguish the weakest bond in Te(3,1) from the rest (bottom third panel in Figure 3d); the latter observation is the electronic-structure signature which supports the preferential weak axial-bond formation with Te(3,1) units (Figure 2e). Several pieces of evidence indicate that the lone pairs of Te(2,2) behave differently from the other lone pairs (bottom two panels of Figure 3d), being more localized at the corresponding central atoms (Figure S5, Supporting Information). The asymmetric (Figure 1a) and delocalized lone-pair MLWFs (Figure S5, Supporting Information) of Te(2,2), along with the shift of the corresponding WFCs (Figure 2h) toward neighboring atoms, indicate that they interact more closely with neighbors than other lone pairs, explaining the resemblance of their $PDOS_{LP}$ to the $PDOS_{BO}$ of weak axial bonds. The PDOSs projected onto MLWFs, hence, clearly differentiate axial and tetrahedral bonding from others, as well as the lone pairs of Te(2,2), in terms of their local electronic structures.

The existence of hypercoordinated atoms means that the 8-N rule[29] is not strictly obeyed in amorphous GST. Nevertheless, the partitioned charge densities (Bader charge[30]) for each type of element with different CNs (and lone pairs) show only a small difference (Figure 3f), which can, in general, be accounted for in terms of polar covalency. For hypercoordinated Sb atoms, i.e., Sb(4,1) or Sb(5,1), the axial bonds show a larger charge shift toward the more electronegative Te ligands than the equatorial (or central) bonds (Figure 3b), such that the total number of electrons on the central antimony atom becomes rather insensitive to the number of ligands. A large degree of polar covalency is, hence, another characteristic of axial bonds. On the other hand, Ge(4,0) units contain slightly more Bader charge than other Ge units (Figure S6, Supporting Information) due to their less polarized bonds (Figure 3b).

So far, we have studied the static atomic structure of amorphous GST models. We now discuss the correlation between chemical bonding and ultrafast crystal-growth processes occurring in GST. **Figure 4**a shows a snapshot taken during annealing simulations for GST (see the Supporting Information). The generated crystalline phase has a (distorted) rock-salt structure,[31] with vacant sites being distributed inside, corresponding to the expected crystalline structure of GST.[32] Perhaps due to the system size, the simulated crystal-growth speed (≈10 m s^{-1}) is of the same order as, but seemingly slightly higher than, the experimental estimation.[33] The populations of some of the major structural units are summarized in Figure 4b (Supporting Information). Many new structural units appeared in comparison with the relaxed amorphous models; these may be considered as thermally transient units. The dynamics of interunit transitions in the amorphous region are illustrated in Figure 4c–e. The electronic configuration of structural units has evolved very quickly via active interunit transitions, as evidenced from their short lifetimes (see Figure S7, Supporting Information). Forward and backward transition rates, defined as the number of interunit transitions per ps per atom (see the Supporting Information), are similar for relevant pairs of units. The transient units are less stable than others. In addition, in accord with the strength of bonding interactions (Figure 3a), hypercoordinated units live less long than (3,1) units, while Ge(4,0) shows the longest mean lifetime among Ge units. In the course of crystal growth at the interface (from top to bottom in Figure 4b), the transition rate is no longer equal for both directions, but is higher for transitions to (3,1) or hypercoordinated units, whose structures are compatible with the cubic crystalline phase. Some of the characteristic features observed during the crystal-growth process are: (i) hypercoordinated units increased at the expense of less coordinated ones by forming more (weak) axial bonds; (ii) tetrahedral Ge(4,0) units diminished significantly during crystal growth, while transforming to hypercoordinated Ge(4,1) or Ge(3,1). This transformation has the effect of preventing incompatible tetrahedral units from being incorporated into the crystalline phase, which

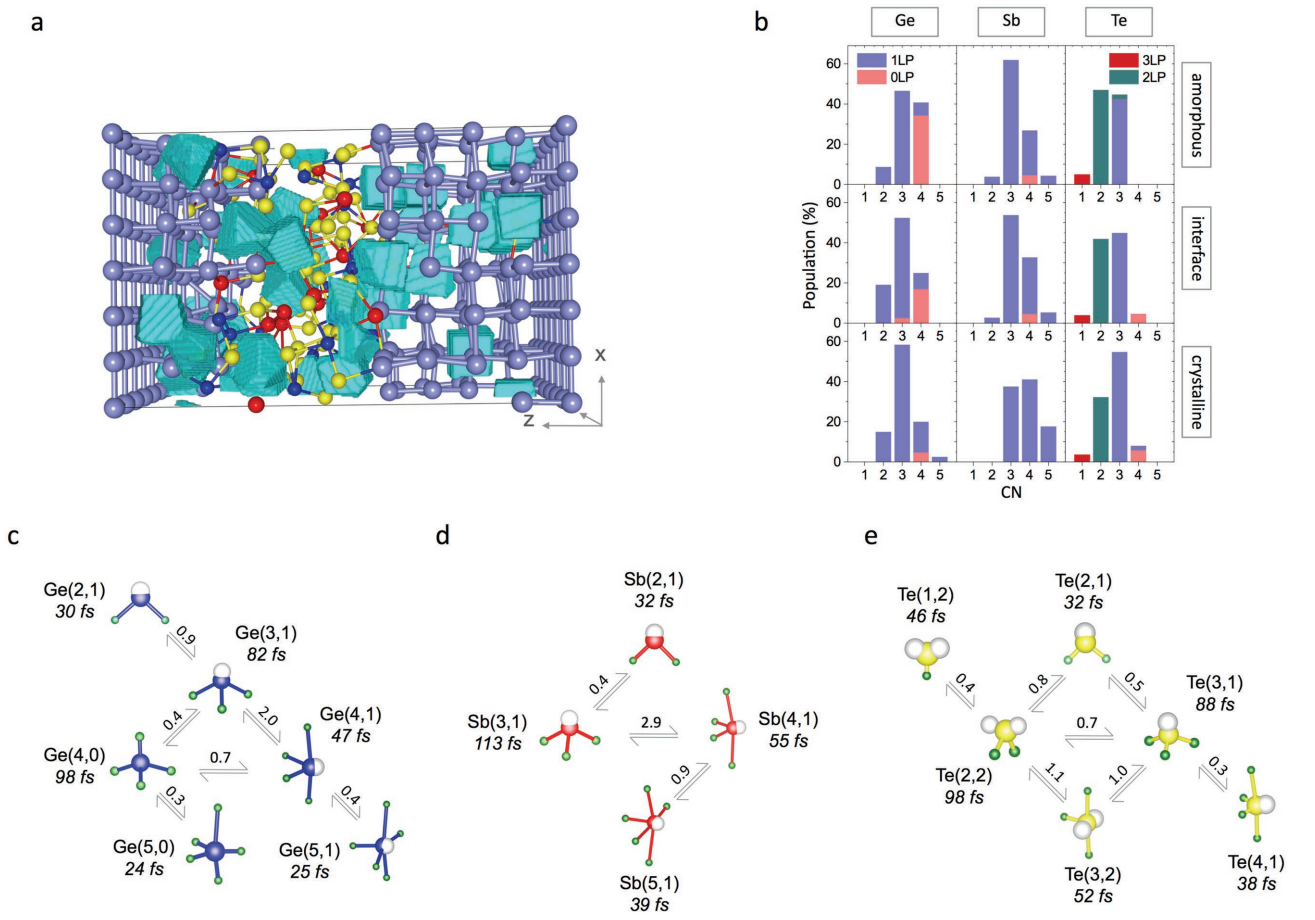

Figure 4. Dynamics of structural units. a) Snapshot of a crystal-growth simulation model. The distribution of Ge (blue), Sb (red), and Te (yellow) atoms, as well as vacant volumes (cyan), are shown. All atoms in the crystalline phase or at the amorphous–crystalline interface are depicted in light blue for clarity. b) Population of structural units with different coordination numbers and number of lone pairs in amorphous or crystalline phases or at the interface. c–e) Interunit transitions between structural units in the amorphous region at 600 K. The mean lifetimes (±8 fs) of Ge (c), Sb (d), and Te (e) structural units and transition rates between them are denoted. Here, the transition rate is defined as the number of interunit transitions per ps per atom of the same species observed in the amorphous region.

otherwise would raise the system energy; and (iii) the lone pairs of Te(2,2) were actively involved in transforming to Te(3,1) units, either via direct additional (often axial) bond formation, or through the transient unit Te(3,2), as shown in Figure 4e. (i) and (iii) are closely related (in agreement with the implication of the electronic-structure results in Figure 3d), underlining the role of weak bonds and lone pairs for fast interunit transitions. A general conclusion, drawn from the short lifetimes and diverse transition pathways (Figure 4c–e), is that units are "structurally flexible" in transformation.

Perhaps the most significant consequence of the presence of "structurally flexible" structural units is the ultrafast crystal-growth kinetics of GST, resulting from sequential, cooperative structural-ordering processes among a group of chemically linked atoms. **Figure 5** illustrates an example of such phenomena observed during crystal-growth simulations; the movement of the indexed atom **1** to its crystalline site (see Figure S10, Supporting Information) initiated a series of collective movements toward crystallization in chronological order, as indicated by the indexed numbers. One of the largest displacements (see Figure 5b) is made by atom **6**, whose movement had been triggered by simultaneous bond breakages between atoms **3**–**2** and **3**–**5**, resulting in triggering, in turn, the crystallization of other atoms **4**, **5**, and **5'**. The two most important factors enabling such a concurrency in crystallization are that: i) large vacancies allow enough space for their collective bonding reconfiguration (Figure 5c); and, more importantly, ii) the "flexible" units could easily transform from one to another (Figure 5d,e) that fit in the crystalline structure (i.e., mostly (3,1)-type or hypercoordinated units) through the mechanisms explained in Figure 4c–e. The number of atoms involved in such simultaneous local crystal growth varied from 2 to ≈10 in our simulations; however, single-atom-involved crystallization was much less frequently observed. The crystal-growth mechanism of GST is, therefore, not simply describable by an individual atomic diffusion process; rather, one should consider collective atomic movements to understand the fast crystallization kinetics of GST. The crucial role of "flexible" structural units for fast crystal-growth processes may be highlighted by a comparison with amorphous silica (a-SiO_2), whose maximum crystal-growth rate is about nine orders of magnitude lower than that observed in GST;[33] the structural units of SiO_2

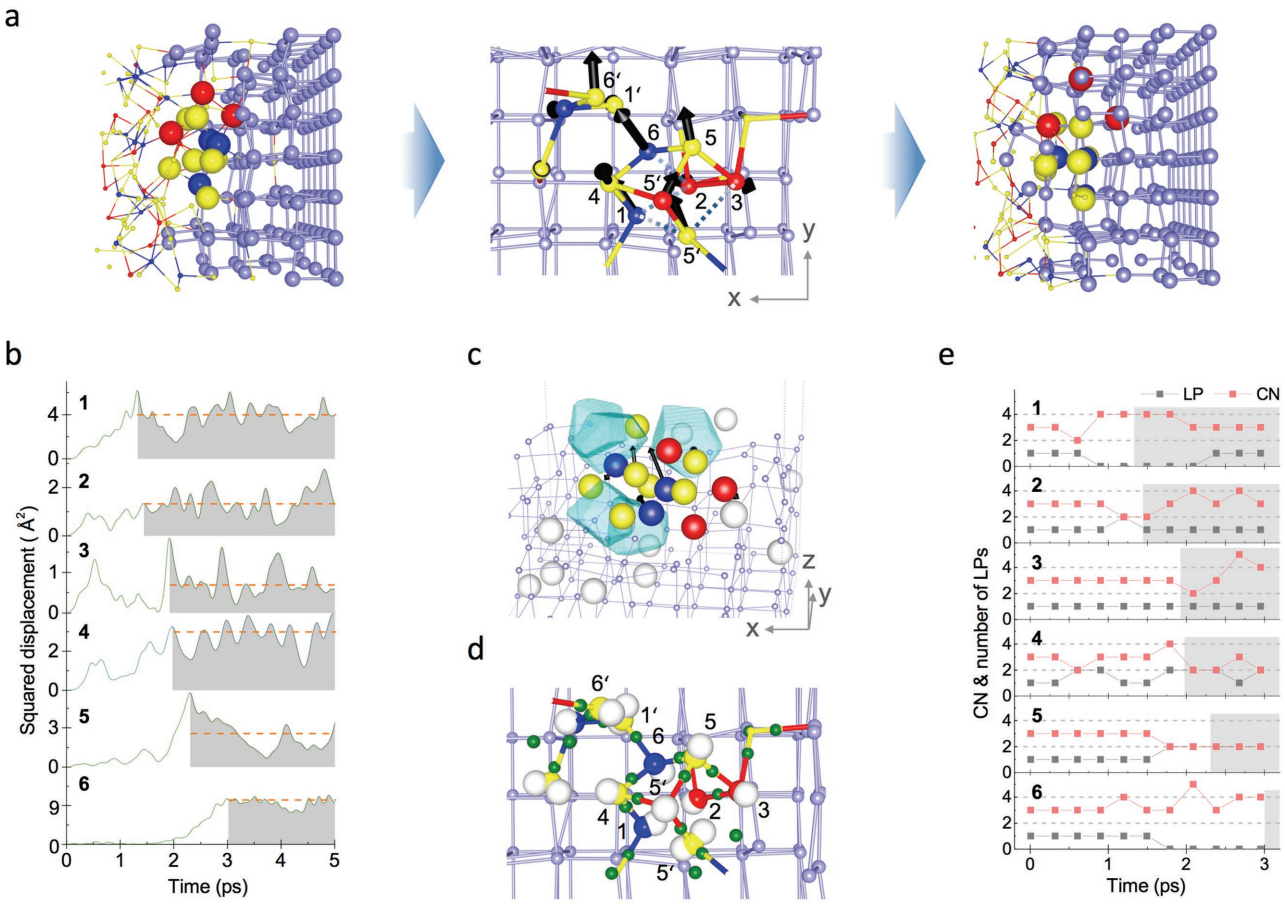

Figure 5. Mechanism of ultrafast crystal growth in GST. a) Sequential, cooperative motions of atoms during crystal growth. Atoms in the amorphous phase (left) diffused to the crystalline-phase interface and crystallized region (right) through their cooperative motions in chronological order, as indicated by the indexed numbers (middle) (same color coding as in Figure 4a). b) Time dependence of squared displacements of the indexed atoms during crystal growth. The simulation time was arbitrarily set to zero for the configuration (left) in (a). The gray areas under the curves indicate that atoms are in their crystalline sites during this time period of simulation. c) Vacant volumes (cyan) near the indexed atoms and atomic movements during cooperative crystallization (indicated by arrows in black). The large balls (white) represent other vacant sites in amorphous or crystalline phases. d) Bond (green) and lone-pair (light grey) MLWF centers for the indexed atoms before their structural ordering. e) Time evolution of coordination numbers and the number of lone pairs for the indexed atoms, sampled during crystal growth.

(mostly tetrahedral SiO_4 units) are "rigid" even at high temperatures (Figure S8, Supporting Information). Although we have primarily focused on bonding configurations leading to fast crystallization in GST, the role of tetrahedral Ge(4,0) units is expected to be different, considering that their molecular symmetry is incompatible with the pseudocubic crystalline phase, together with their relatively strong bonding interactions and long lifetimes, in contrast to hypercoordinated units. However, whether or not Ge(4,0) units work as a supposed slowing-down element against structural ordering is not certain from our simulations; the bonding characteristics of Ge(4,0) units, similar to those of tetrahedrally coordinated "retarding" dopants in GST,[34] and experimental observations, such as an increase in thermal stability with more Ge in Ge-Sb-Te systems,[35] may indicate that, to a certain extent, Ge(4,0) units play an opposite role to that of other units.

In conclusion, the local atomic structure of a-GST is very complicated. This structural complication is a manifestation of diverse permitted electronic configurations, allowing for facile local-structural changes (or valence-charge redistributions) leading to fast crystallization at high temperatures; the weak bonds, as well as (correlated) lone pairs, play a role in alleviating the energetic cost associated with bond breakage, and in providing a convenient route for bond reformation. The resultant cooperative-crystallization processes give rise to the ultrafast crystal growth observed in GST. Since most other well-known PCMs are also lone-pair-rich Te-based chalcogenides, the current study may provide a universal explanation for the unique crystallization kinetics of such PCMs, while offering an exciting opportunity to investigate various other dynamical properties of PCMs, or of other glasses, from the point of view of local electronic structures and their dynamical behavior.

Supporting Information

Supporting Information is available from the Wiley Online Library or from the author.

Acknowledgements

The authors acknowledge financial support from the Engineering and Physical Sciences Research Council (UK). The AIMD simulations were partially performed using the Cambridge High-Performance Computing Facility (Darwin). Some of the raw data discussed in this manuscript is available online from https://doi.org/10.17863/CAM.8695.

Conflict of Interest

The authors declare no conflict of interest.

Keywords

chemical bonding, crystal growth, DFT calculations, phase-change materials

Received: February 9, 2017
Revised: March 7, 2017
Published online:

[1] S. R. Elliott, *Nature* **1991**, *354*, 445.
[2] W. H. Zachariasen, *J. Am. Chem. Soc.* **1932**, *54*, 3841.
[3] M. Wuttig, N. Yamada, *Nat. Mater.* **2007**, *6*, 824.
[4] D. Loke, T. H. Lee, W. J. Wang, L. P. Shi, R. Zhao, Y. C. Yeo, T. C. Chong, S. R. Elliott, *Science* **2012**, *336*, 1566.
[5] S. R. Ovshinsky, *Phys. Rev. Lett.* **1968**, *21*, 1450.
[6] D. Kuzum, R. G. D. Jeyasingh, B. Lee, H.-S. P. Wong, *Nano Lett.* **2012**, *12*, 2179.
[7] T. H. Lee, D. Loke, W. J. Wang, K. J. Huang, S. R. Elliott, *Adv. Mater.* **2014**, *26*, 7493.
[8] J. Akola, R. O. Jones, *Phys. Rev. B* **2007**, *76*, 235201.
[9] J. Hegedus, S. R. Elliott, *Nat. Mater.* **2008**, *7*, 399.
[10] T. H. Lee, S. R. Elliott, *Phys. Rev. Lett.* **2011**, *107*, 145702.
[11] M. M. J. Treacy, J. M. Gibson, L. Fan, D. J. Paterson, I. McNulty, *Rep. Prog. Phys.* **2005**, *68*, 2899.
[12] R. T. Sanderson, *Polar Covalence*, Academic Press, New York **1983**.
[13] R. J. Gillespie, I. Hargittai, *The VSEPR Model of Molecular Geometry*, Allyn and Bacon, Boston, MA, USA **1991**.
[14] M. Xu, Y. Q. Cheng, H. W. Sheng, E. Ma, *Phys. Rev. Lett.* **2009**, *103*, 195502.
[15] A. V. Kolobov, P. Fons, J. Tominaga, *Sci. Rep.* **2015**, *5*, 13698.
[16] T. H. Lee, S. R. Elliott, *Phys. Rev. B* **2011**, *84*, 094124.
[17] F. Zipoli, D. Krebs, A. Curioni, *Phys. Rev. B* **2016**, *93*, 115201.
[18] A. D. Becke, K. E. Edgecombe, *J. Chem. Phys.* **1990**, *92*, 5397.
[19] N. Marzari, A. A. Mostofi, J. R. Yates, I. Souza, D. Vanderbilt, *Rev. Mod. Phys.* **2012**, *84*, 1419.
[20] G. Kresse, J. Hafner, *Phys. Rev. B* **1993**, *47*, 558.
[21] P. L. Silvestrelli, N. Marzari, D. Vanderbilt, M. Parrinello, *Solid State Commun.* **1998**, *107*, 7.
[22] A. Savin, R. Nesper, S. Wengert, T. F. Fassler, *Angew. Chem., Int. Ed. Engl.* **1997**, *36*, 1808.
[23] R. F. W. Bader, *Atoms in Molecules*, Oxford University Press, New York **1990**.
[24] R. J. Gillespie, R. S. Nyholm, *Q. Rev., Chem. Soc.* **1957**, *11*, 339.
[25] R. Hoffmann, *Solids and surfaces: A Chemist's View of Bonding in Extended Structures*, VCH, Weinheim, Germany **1988**, p. 43.
[26] J. P. Perdew, K. Burke, M. Ernzerhof, *Phys. Rev. Lett.* **1996**, *77*, 3865.
[27] J. Heyd, G. E. Scuseria, M. Ernzerhof, *J. Chem. Phys.* **2003**, *118*, 8207.
[28] A. V. Kolobov, P. Fons, J. Tominaga, *Phys. Rev. B* **2013**, *87*, 155204.
[29] N. F. Mott, *Philos. Mag.* **1969**, *19*, 835.
[30] W. Tang, E. Sanville, G. Henkelman, *J. Phys.: Condens. Matter* **2009**, *21*, 084204.
[31] A. Lotnyk, S. Bernutz, X. Sun, U. Ross, M. Ehrhardt, *Acta Mater.* **2016**, *105*, 1.
[32] N. Yamada, T. Matsunaga, *J. Appl. Phys.* **2000**, *88*, 7020.
[33] J. Orava, A. L. Greer, *J. Chem. Phys.* **2014**, *140*, 214504.
[34] T. H. Lee, D. Loke, S. R. Elliott, *Adv. Mater.* **2015**, *27*, 5477.
[35] N. Yamada, E. Ohno, K. Nishiuchi, N. Akahira, *J. Appl. Phys.* **1991**, *69*, 2849.